Nuclear Materials and Energy 38 (2024) 101628

Contents lists available at ScienceDirect

Nuclear Materials and Energy

journal homepage: www.elsevier.com/locate/nme

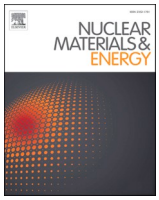

Effects of beam scanning modes on ion-irradiated iron microstructure

T. Dunatov [a,*], M. Roldan [b], T. Tadić [a,*]

[a] Ruđer Bošković Institute, Zagreb, Croatia
[b] CIEMAT, National Fusion Laboratory, Technology Division, Madrid, Spain

ARTICLE INFO

Keywords:
Ion beam irradiation
Scanning
Dose rate
Void formation
Iron

ABSTRACT

Neutron induced damage in future nuclear materials can be studied using heavy ion beams only if the differences in the microstructure evolution are well understood. Large variations in the damage dose rate, caused by scanning of the ion beam, can alter the microstructure compared to steady-state irradiation. We study the effect of scanning on the microstructure by irradiating pure iron with a 10 MeV Fe ion beam to a dose of 0.2 dpa. The beam is scanned in one direction with frequencies of 200 Hz and 10 kHz. Different shapes of the beam are also used to study the effect of dose variation. All of the irradiations are conducted at room temperature using the DiFU chamber at RBI. TEM analysis shows differences between the narrow beam and defocused irradiation modes, including unusual void formation observed at 10 kHz. A wider beam reduces the effect of scanning speed and no voids are found in this scanning case.

1. Introduction

The development of future fusion power plants requires an extensive database of material behavior under neutron radiation and the resulting radiation damage [1]. Experiments under such conditions have not been technically feasible so far due to the lack of an intense fusion neutron source such as IFMIF-DONES [2 3]. Heavy ion irradiation in the MeV range, either in single beam or dual beam mode, is among the methods used to study defects generated in these conditions [4 5]. This method enables significant doses to be achieved within several days, though it requires accounting for differences in fundamental physics and a limited analysis area.

The dose rate in ion irradiation experiments, measured in dpa/s (displacements per atom per second), is larger than that of a typical reactor environment by one to two orders of magnitude [5]. To obtain a uniform dose over the sample surface, so called scanning or rastering of the beam over the sample surface is often employed. In this way a further increase in the instant dose rate is created, as well as large variations in the dose rate over time. Though in some designs fusion reactors operate in pulsed mode such dose rate variations are in general considered to be neutron atypical and they have the potential to affect the evolution of microstructure under irradiation [6].

A few studies of this rastering or pulsing effect have been conducted comparing the microstructure obtained with a scanned beam to that obtained with the constant beam or "defocused" irradiation mode [7 8 9]. Lee et al. [7], investigated pulsing effects with periods of 60 s and 1 s in a Ni irradiated austenitic stainless steel alloy. Low (1 dpa) and high (70 dpa) dose samples irradiated at high temperature with and without helium co-injection exhibited reductions in size of both interstitial loops and voids when pulsing. This was attributed to the pulsing period being comparable to the vacancy lifetime of < 1 s. Getto et al. [8] conducted a similar study of Fe irradiated iron alloys pre-implanted with different quantities of He and observed similar suppression of microstructural evolution when scanning. In the discussion it is suggested that raster scanning at frequencies of over 500 Hz with the experimental conditions shown should eliminate pulsing effects. Finally, and most similar to the present study, Gigax et al. [9] irradiated pure iron at frequencies of 0.244, 1.94 and 15.6 Hz, as well as with a defocused beam at 450 °C. The scanning in all cases showed a reduction in the void swelling compared to the defocused case, and the swelling further decreased with an increase in scanning frequency. Such a decrease is explained by the vacancy emission during the beam-off period. Similar studies in tungsten, another fusion-relevant material, report variation of the microstructure depending on the dose rate [10 11], but no difference in deuterium retention depending on the dose rate or irradiation mode [12].

Scanning of the beam is essentially pulsing on a microstructural level. Related research in semiconductors involves the use of pulsing beams to study defect diffusion in cascades [13 14]. Here it is found that the disorder, i.e. damage, as measured with RBS in channelling mode, depends on the pulsing rate of the beam. Based on the available data the

* Corresponding authors.
E-mail addresses: Toni.Dunatov@irb.hr (T. Dunatov), Tonci.Tadic@irb.hr (T. Tadić).

https://doi.org/10.1016/j.nme.2024.101628
Received 30 November 2023; Received in revised form 15 February 2024; Accepted 28 February 2024
Available online 1 March 2024

ASTM E521-16 [15] standard currently recommends to use a defocused beam spot in ion irradiations of nuclear materials with a small amount of homogenization ("wobbling") [5] if needed.

From a theoretical point of view, the generation and destruction of defects in time can be modelled with kinetic rate theory for which detailed work exists [6 16 17 18]. More recently simple models which describe a radial diffusion of the defects from the cascade have been shown to align with the experimental data [11 13]. In the limiting case of very fast pulsing (i.e. high scanning frequencies) it is predicted that the defect evolution would proceed as in the continuous case.

However, to our knowledge no studies have been conducted of the effect of scanning frequencies in the 10 kHz range or of the effects of beam shape. The purpose of this work is a further investigation of the microstructural effects of beam scanning as a study of the best practices of ion irradiation. We investigate different beam spots, shown schematically in Fig. 1 and scanning frequencies of 200 Hz and 10 kHz as well as a static beam. We refer to these beam spot shapes as the narrow beam, wide beam, and defocused beam, respectively.

2. Methods

The study focuses on high-purity iron, produced under contract EFDA-06–1901. The iron was processed to achieve a recrystallized state through a 70 % cold reduction and subsequent heat treatment at 700 °C for an hour, followed by natural cooling. Details about the alloy chemical composition, the average grain size post heat treatment and dislocation density can be found elsewhere [19 20]. The distribution of these dislocations was found to be uneven across the sample, although the density was very low. Before irradiation, 1 cm discs were cut from a cylinder using a slow-speed diamond saw, polished using the conventional route to a mirror finish, and electropolished with Struers' LectroPol using a sulfuric acid and methanol solution (4:1) at 15 °C. Subsequently, they were ultrasonically cleaned in pure ethanol to avoid oxidation phenomena. Self-ion irradiations were conducted at RBI in the DiFU chamber of the Laboratory for ion beam interactions [21] using a 10 MeV Fe^{3+} beam obtained from the Tandem Van de Graaff accelerator. The beam's energy is determined using a 90° analyzing magnet. To obtain the desired shape and size of the stationary beam magnetic quadrupole focusing is used. Scanning is then conducted using Danfysik electrostatic scanning plates connected to high frequency Matsusada amplifiers. The amplifiers obtain an input triangle wave signal from a custom made scanning board, and amplify it to up to a voltage of ± 10 kV. An oscilloscope was used to check the correct shape and frequency of the amplifier signal. The shape of the irradiation spot is determined by a slit system, and the current measurement is made using a Faraday cup with a secondary electron suppression electrode. Plasma cleaning before and after the irradiations and a liquid nitrogen cold trap were employed in order to minimize the carbon build-up [22]. A residual gas analyzer was also employed during the entire experimental process. The vacuum during the experiment remained on the order of 10^{-8} mbar with no high mass impurities corresponding to carbon. Further details regarding the experimental chamber can be found in a separate reference [21].

The damage profile is given in Fig. 2. It is calculated with SRIM using the Kinchin-Pease method and a displacement energy of 40 eV [23]. The 0.2 dpa value stated refers to the average of the damage along the first micrometer of the sample. This is the main area of interest in order to avoid the injected interstitial effect and ensure a mostly uniform damage profile. The recommendation to use the KP method is based on inconsistencies found in the Full Cascade calculation, which claims to be the more accurate method [23]. Recently the IRAD code [24], a modification of Iradina [25], was published which resolves these inconsistencies. With this code in the full cascade mode we obtain an approximately 25 % larger damage, i.e. 0.25 dpa. Both profiles are reported in Fig. 2 along with the ion fluence of 1.1 x 10^{15} ions/cm^2 for reference.

The defocused beam was made by spreading the beam spot over a wide area using the quadrupoles and then cutting the edges with the slit system. Two different types of scanned beam spot were used, a narrow spot of 1 mm FWHM of the size typically used for scanning and a "wide beam" approximately 7 mm in FWHM. Scanning of the beam was conducted only in the horizontal direction to simplify the analysis, a scanning area of 1x1 cm^2 was defined using the slit system to cover the entire sample. The frequency is defined using a custom-made program which defines the scanning over a certain number of pixels. Both the dwell time per pixel and total number of pixels can be adjusted. The values of the dwell time for different frequencies are given in Table 1. Scanning was conducted over 10 evenly spaced pixels for all of the scanned irradiations. The frequency is therefore equal to $f = 1/10T_d$, where T_d is the dwell time. For the narrow beam spot the beam-on time is taken to be identical to the dwell time, while the beam-off time is the remaining time of the scanning period. This would not be an accurate picture for the wide beam case as in this case the size of the beam spot is comparable to the size of the irradiation area. Therefore, for the WB10000 sample the beam-on and beam-off times of 70 μs and 30 μs are estimated as the time spent inside and outside the 7 mm FWHM of the beam during a scan. In this way the values remain consistent with those reported in the narrow beam case. However, it needs to be emphasized that the dose rate is never exactly zero in this case as shown in Fig. 1.

Shapes of the beam were adjusted using a scintillating quartz. The profile of the wide beam was measured also with the custom made beam profile monitoring system as described in [21] and shown in Fig. 1. With the wide beam case a static beam irradiation (without scanning) was also made as a control. All of the experiments were made at room temperature. Potential beam heating was monitored by an IR camera

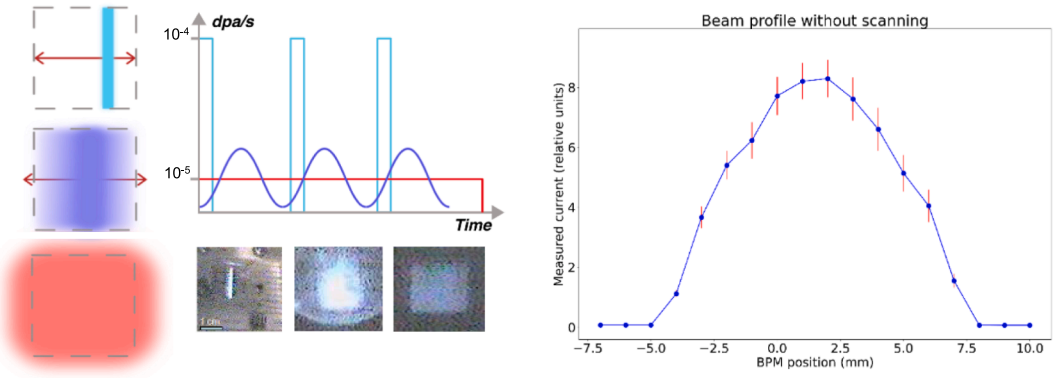

Fig. 1. Left - schematic depiction of the dose rate with different beam shapes used and their image on the scintillating quartz. Right – the wide beam shape as measured on the beam profile monitoring system [21].

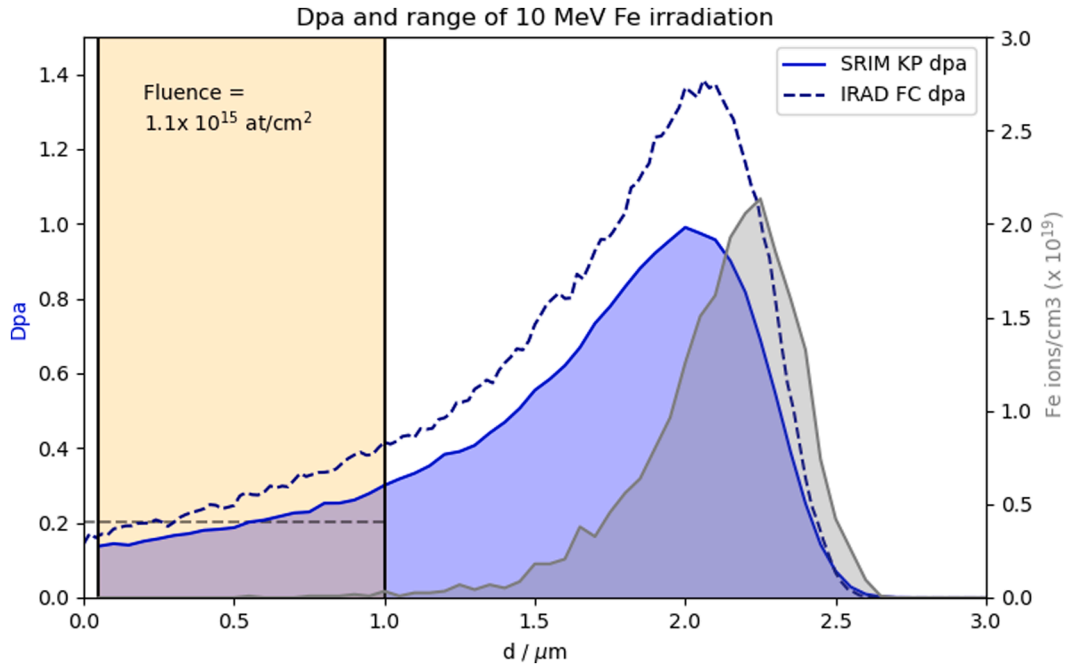

Fig. 2. Dpa and ion implanted concentration inside the sample.

Table 1
The scanning parameters of the samples analyzed. The average dose rate is approximately the same for all samples, but the peak dose varies due to the scanning effect, as shown schematically in Fig. 1.

Sample	Description	Pixel dwell time (μs)	Beam-on time (μs)	Beam-off time (μs)	Peak dose rate (dpa/s)
LD0	(defocused)	∞	∞	∞	2.4×10^{-5}
LD200	(200 Hz narrow beam)	500	500	4500	2.4×10^{-4}
LD10000	(10 kHz narrow beam)	10	10	90	2.4×10^{-4}
WB static	(wide beam)	∞	∞	∞	3.9×10^{-5}
WB10000	(10 kHz wide beam)	10	70	30	3.9×10^{-5}

and a thermocouple mounted on one of the samples. Neither the camera nor the thermocouple detected significant heating, with the maximum temperature recorded being 34° C.

S/TEM analysis of the irradiated materials required the extraction of lamellae, approximately 5 x 4 μm in size and 50 nm thick, from areas of interest regarding the material's response. Conducted at the University of Zaragoza's Advanced Microscopy Laboratory (LMA, Zaragoza, Spain), a Helios 600 Dual Beam microscope facilitated the sample preparation. The protocol began with an electron beam-deposited platinum protective layer (1.4 μm thick, 12 x 1 μm area) at 30 kV and 93 pA. Subsequent rough thinning by a Gallium ion beam defined two trapezoidal sections flanking the platinum, progressing to a 1 μm thickness. The platinum-welded lamellae were then secured onto a copper TEM grid. The final thinning, cautious to prevent over-reduction and potential microstructural alteration, was performed at low beam currents and polished with voltages down to 2 kV, including a grid rotation for uniformity. The final step consisted in a Low Ar kV ion polishing, using PIPS. Observations of these lamellae utilized a 200 kV JEOL 2100HT and a JeolTEM/STEM 3000F, at CNME (Complutense University of Madrid, Spain).

3. Results and discussion

Most radiation-induced defects appear as black dots several nanometers in diameter (Fig. 3 and Fig. 4). These are embryo-type dislocation

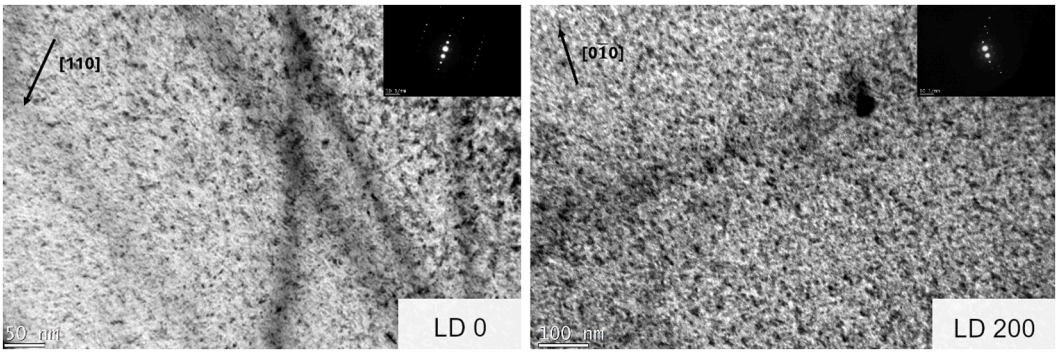

Fig. 3. TEM images of different samples showing "black dot" type defects using a defocused beam (left) and rastered at 200 Hz (right).

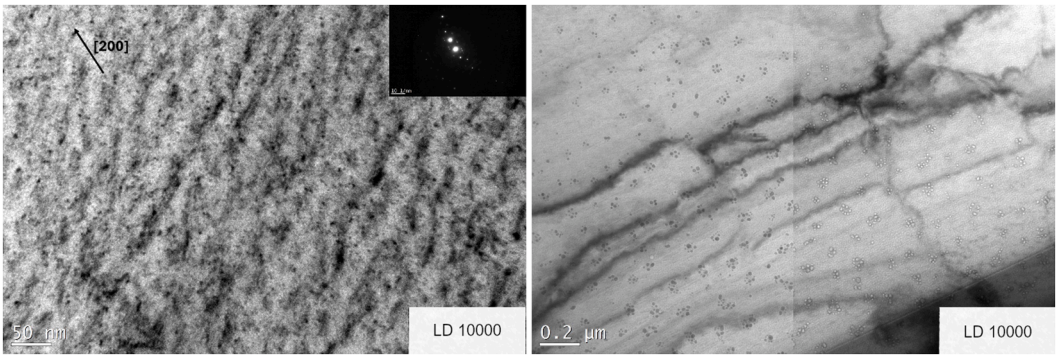

Fig. 4. TEM images of the LD10000 sample. Left – the black dot type dislocation defects are visible. Right – Image of the voids observed in the 10 kHz narrow beam irradiated sample. Overfocused (black contrast) and underfocused (white contrast) micrographs.

loops (also known as black dots) too small to determine their burger vector just analyzing the shape and knowing the habit plane as published in [26]. It is well known that at room temperature the point defects are not sufficiently mobile to cluster into larger dislocations, so they create the initial state of eventual loops. Pinning of the dots to mechanically induced dislocations is also observed. Surprisingly, on the sample irradiated at 10 kHz void formation was also discovered as seen in Fig. 4.

Voids are observed in clusters, seemingly aligned along crystallographic planes. Similar behavior is seen in irradiations conducted under strain [27]. Such a partially ordered microstructure also resembles so-called void super-lattices. These are highly ordered lattices of defects which are found under certain conditions, generally having the same lattice structure as the metal itself [28 29]. Quantitative analysis of the defect sizes was performed manually using the ImageJ software package [30]. The distribution of sizes was compared for images of similar resolution (~3 pixels/nm) to ensure consistency in the measurement. For each image the counting was also divided in several sections, to confirm there is no significant variation in defect size between them. Histograms of the black dot distributions are shown in Fig. 5. In the defocused case, defects are on average 3.4 nm in diameter. For the narrow beam scanning mode an increase of the average size of defects to approximately 4 nm is observed in the 200 Hz scanning regime as well as a wider distribution of defect diameters. Increasing the scanning frequency to 10 kHz reduces the average defect size to a value of approximately 3.3 nm, with a distribution close to the defocused case.

The distribution of voids peaks at an average diameter of 12 nm, with the voids clustering together in groups of several as seen in Fig. 4. Larger voids seem to be formed by the smaller ones combining.

Due to these unexpected results, STEM was also conducted to confirm that the results are independent of the specific diffraction conditions used in TEM. Indeed, it was confirmed that the defects are randomly distributed without preferential ordering. Because of the simpler interpretation STEM images were chosen as more suitable for the analysis in the wide beam case (Fig. 6). The microstructure is similar with all three samples studied, with the only notable difference being the smaller standard deviation of the wide static beam case. No void formation is observed in any of the wide beam irradiated samples. This seems to indicate that the wide beam "wobbling" indeed reduces the scanning effect as assumed.

The wider distribution of defect sizes when scanning can be explained by the fluctuation in the dose rate during irradiation. A cascade diffusion theory [31] predicts that the variance of the number of defects collected by a cluster is a function of the defect diffusion time, which depends on the dose rate. This variance becomes especially significant for damage production in timescales on the order of the defect diffusion time.

Previous studies have shown a decrease in defect size with the scanning beam, opposite to that found here. However, those studies were conducted at high temperature conditions, where vacancies are more mobile. For instance, Lee et al. [7] suggest that the decrease in loop size occurring at 1 dpa is a result of the residual vacancies from the damage pulse arriving at dislocation loops during the beam-off time. The low vacancy mobility at room temperature should reduce this effect. Apart from the beam-off annealing, differences in dose rate should also be considered, as the narrow beam scanned case has a larger instant dose rate. One should therefore expect a larger equilibrium concentration of defects during each scanning pulse. This should be the case for both the

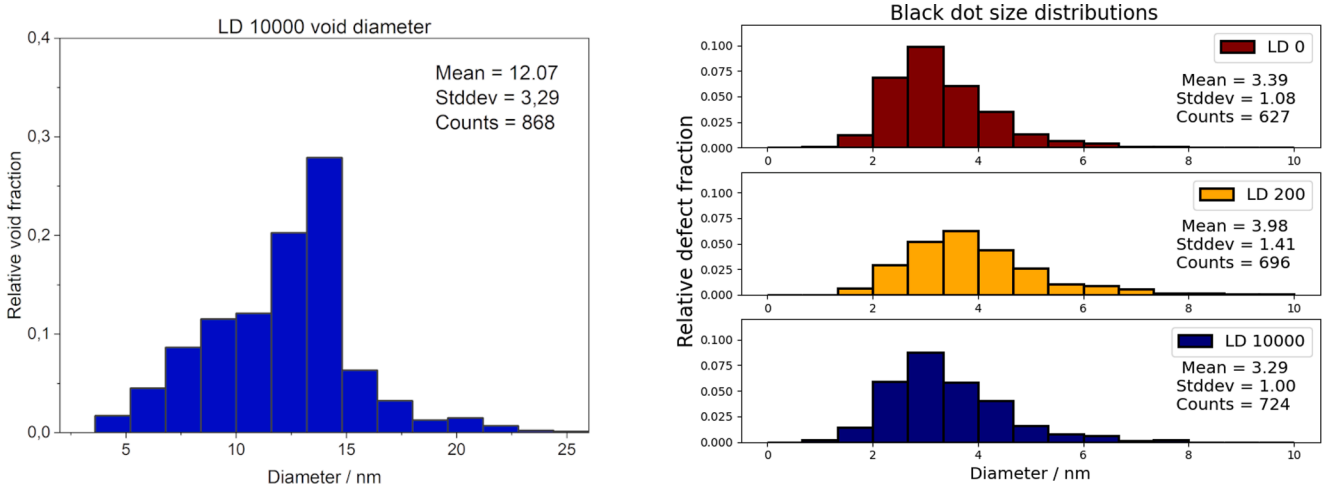

Fig. 5. Distributions of voids and black dot type defects in the narrow beam irradiated samples.

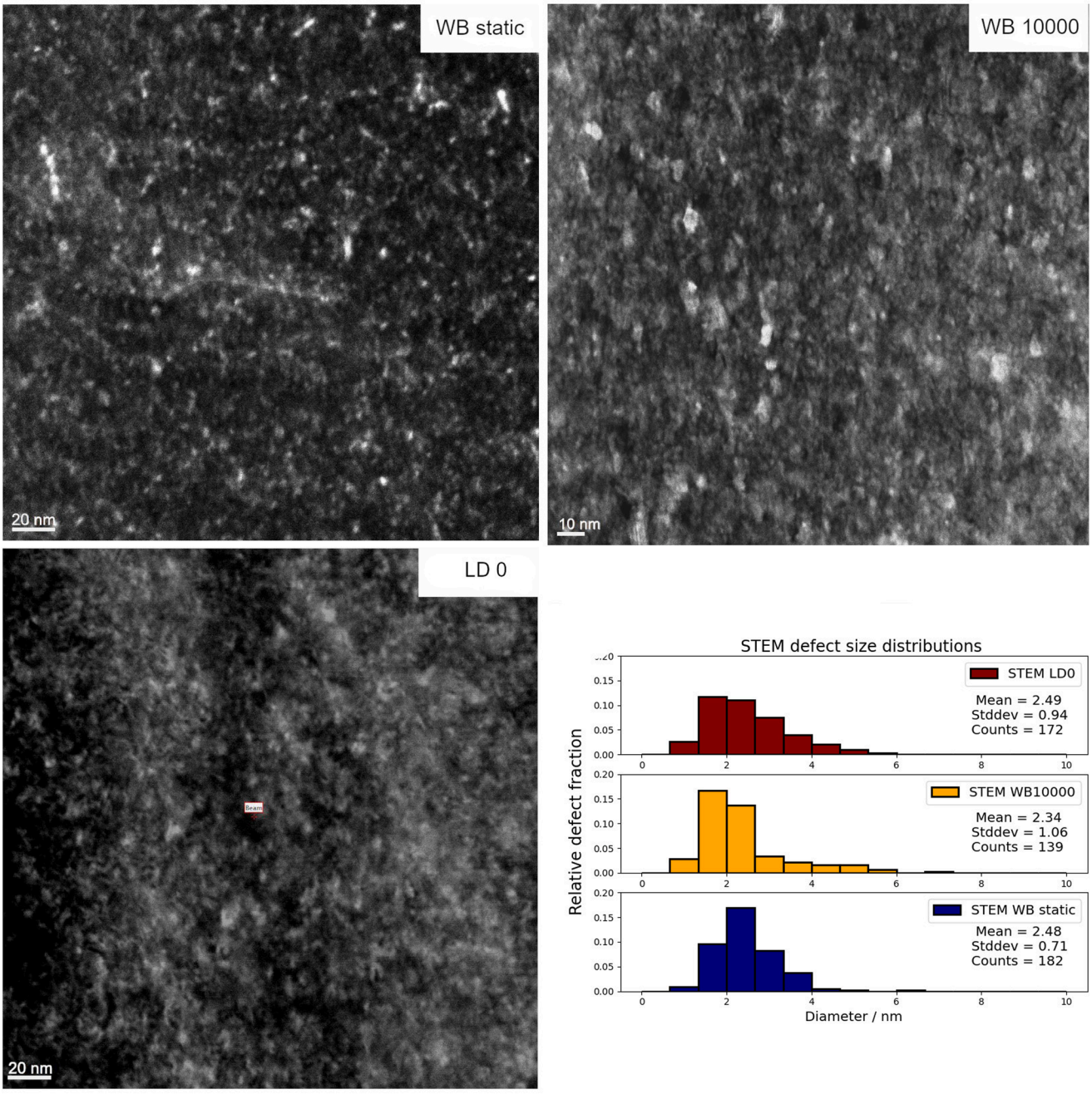

Fig. 6. STEM images of the wide beam samples compared to the defocused irradiated sample, along with the distribution of defect sizes.

200 Hz and 10 kHz samples, however it is possible that the high frequency pulsing does not reach an equilibrium state as will be discussed later.

The void formation is very unexpected as the vacancies at room temperature should not be sufficiently mobile to cluster into voids. In the low dose and low temperature regime recombination of vacancies and interstitials is expected to be the dominant interaction. While it is possible that the narrow beam causes an instant local increase in the temperature of the sample, such an increase would also be observed in the sample irradiated at a lower frequency and the heating effect should in fact be larger there.

Nucleation of voids can also be precipitated by impurities such as carbon which is known to build-up in iron in ion-irradiation experiments [32 33]. However, contamination mitigation methods ensured that the vacuum was of high quality throughout and indeed EELS measurements conducted alongside STEM found no significant contamination. The possibility of carbon or other elements being included as an impurity in the beam itself was excluded in previous tests [21], as no such impurities were found deep in the samples and the 90° analyzing magnet provides good filtering of the ion beam. Finally, since several samples were mounted in the chamber at the same time, any contamination effect would be seen in more than one sample.

It would therefore seem more likely that the void creation effect is a consequence of the short beam-on time. The characteristic diffusion length of an interstitial during a pulse can be found as $L = \sqrt{D\tau}$, where $D = D_0 \exp\left(-\frac{\Delta E}{kT}\right)$ is the defect diffusion constant and τ the beam-on time. From literature the migration energy of interstitials in pure iron is approximately 0.2 eV [34], taking this value and a value of $D_0 = 1.25$ x 10^{-3} cm^2/s calculated from the Debye frequency and geometric parameters of iron, we obtain values of $L = 23$ nm and $L = 166$ nm for the 10

μs and 500 μs pulses respectively. As stated before statistical fluctuations of defect arrival times at sinks are expected to become important for extremely short pulses. This is stated in [31] as the condition that $\tau \ll \frac{1}{Dk^2}$, where k is the effective sink strength in units of m^{-1}. Short diffusion lengths therefore correspond to non-equilibrium states and large statistical fluctuations.

Detailed rate theory calculations [6 17] take into account all the aspects of defect loss to sinks. By neglecting defect recombination, Gurol and Ghoniem [18] obtain simple expressions which show the growth of the vacancy concentration in time during very fast pulsing. This is caused by the slow diffusion of vacancies, which means that they are not completely lost during the beam-off time. Interstitials, however, are significantly more mobile and are quickly lost to sinks so that they never increase above the equilibrium value. The literature regarding defect super-lattice formation [28 29] notes that some vacancy clusters (loops) are formed directly from the collisional cascade (cascade collapse) and it is suggested that this contributes to the super-lattice formation. The incomplete ordering observed here does not exhibit all of the properties of a superlattice, but we believe that this cascade effect could be relevant in the high-frequency results of the present work. We suggest therefore that the void creation and clustering is a combination of the non-equilibrium state of the defects and the cascade collapse effect. A more detailed understanding of the process would require further data at higher doses and temperatures, as well as a more in depth theoretical calculation which is beyond the scope of this paper.

4. Conclusions

In this study, self-ion irradiation of iron to a dose of 0.2 dpa reveals differences in defect evolution depending on the irradiation mode. Key observations include the identification of larger defects and a broader distribution of defect sizes in the low-frequency scanning mode compared to the defocused mode. Notably, the high-frequency (10 kHz) narrow beam scanning mode was associated with the nucleation of large voids, a phenomenon not observed under other irradiation conditions. This suggests that the very short pulsing periods characteristic of high-frequency scanning do not reproduce the constant beam case.

The results seem to qualitatively indicate that the variation of the dose rate induces variation of the defect arrival times and defect growth rate. The very short beam-on time in the 10 kHz narrow beam scanned case is the likely cause of the void nucleation which is not observed in the other samples. Scanning with a narrow beam at high frequency therefore does not reproduce the defocused microstructure at frequencies of this magnitude. Basic defect diffusion length calculations suggest that this is due to the beam-on time which is not large enough to reach an equilibrium state. Our results also suggest that defocused beam scanning, or "wobbling," can mitigate some of the effects seen with narrow beam scanning, producing a microstructure more akin to that observed with defocused irradiation. The implications of these findings can be significant in the context of developing materials for nuclear fusion applications where radiation tolerance is critical, and ion irradiation is one of the methods used.

For future work, we recommend:

- Extending the study to include a broader range of materials, including other metals and alloys more relevant to nuclear applications, to assess the generalizability of our findings.
- Investigating the effects of beam scanning modes at higher doses and temperatures to better understand the mechanisms driving the observed microstructural changes and to explore the potential for tailoring material properties through controlled irradiation strategies.
- Employing advanced modeling techniques to simulate the defect evolution under various irradiation conditions, providing deeper insights into the physical processes at play and guiding experimental efforts.

CRediT authorship contribution statement

T. Dunatov: Writing – review & editing, Writing – original draft, Methodology, Investigation, Formal analysis, Conceptualization. **M. Roldan:** Writing – review & editing, Methodology, Investigation, Formal analysis. **T. Tadić:** Writing – review & editing, Supervision, Methodology, Funding acquisition, Conceptualization.

Declaration of competing interest

The authors declare that they have no known competing financial interests or personal relationships that could have appeared to influence the work reported in this paper.

Data availability

Data will be made available on request.

Acknowledgments

This work has been carried out within the framework of the EUROfusion Consortium, funded by the European Union via the Euratom Research and Training Programme (Grant Agreement No 101052200 – EUROfusion). Views and opinions expressed are however those of the author(s) only and do not necessarily reflect those of the European Union or the European Commission. Neither the European Union nor the European Commission can be held responsible for them.

References

[1] J. Knaster, A. Moeslang, T. Muroga, Materials research for fusion, Nat. Phys. 12 (May 2016) 424–434.
[2] A. Ibarra, F. Arbeiter, D. Bernardi, W. Krolas, M. Cappelli, U. Fischer, R. Heidinger, F. Martin-Fuertes, G. Micciché, A. Muñoz, F.S. Nitti, T. Pinna, A. Aiello, N. Bazin, N. Chauvin, S. Chel, G. Devanz, S. Gordeev, D. Regidor, F. Schwab, The european approach to the fusion-like neutron source: the IFMIF-DONES project, Nucl. Fusion 59 (May 2019) 065002.
[3] J. Knaster, P. Garin, H. Matsumoto, Y. Okumura, M. Sugimoto, F. Arbeiter, P. Cara, S. Chel, A. Facco, P. Favuzza, T. Furukawa, R. Heidinger, A. Ibarra, T. Kanemura, A. Kasugai, H. Kondo, V. Massaut, J. Molla, G. Micciche, S. O'hira, K. Sakamoto, T. Yokomine and E. Wakai, "Overview of the IFMIF/EVEDA project," *Nuclear Fusion,* vol. 57, p. 102016, June 2017.
[4] G.S. Was, Challenges to the use of ion irradiation for emulating reactor irradiation, J. Mater. Res. 30 (April 2015) 1158–1182.
[5] S.J. Zinkle, L.L. Snead, Opportunities and limitations for ion beams in radiation effects studies: bridging critical gaps between charged particle and neutron irradiations, Scr. Mater. 143 (January 2018) 154–160.
[6] E.P. Simonen, N.M. Ghoniem, N.H. Packan, Pulsed flux effects on radiation damage, J. Nucl. Mater. 122 (May 1984) 391–401.
[7] E.H. Lee, N.H. Packan, L.K. Mansur, Effects of pulsed dual-ion irradiation on phase transformations and microstructure in ti-modified austenitic alloy, J. Nucl. Mater. 117 (July 1983) 123–133.
[8] E. Getto, Z. Jiao, A.M. Monterrosa, K. Sun, G.S. Was, Effect of irradiation mode on the microstructure of self-ion irradiated ferritic-martensitic alloys, J. Nucl. Mater. 465 (October 2015) 116–126.
[9] J.G. Gigax, E. Aydogan, T. Chen, D. Chen, L. Shao, Y. Wu, W.Y. Lo, Y. Yang, F. A. Garner, The influence of ion beam rastering on the swelling of self-ion irradiated pure iron at 450 \textdegreeC, J. Nucl. Mater. 465 (October 2015) 343–348.
[10] W. Chrominski, L. Ciupinski, P. Bazarnik, S. Markelj, T. Schwarz-Selinger, TEM investigation of the influence of dose rate on radiation damage and deuterium retention in tungsten, Mater Charact 154 (August 2019) 1–6.
[11] W. Jiang, Y. Zhu, L. Zhang, D.J. Edwards, N.R. Overman, G. Nandipati, W. Setyawan, C.H. Henager, R.J. Kurtz, Dose rate effects on damage accumulation and void growth in self-ion irradiated tungsten, J. Nucl. Mater. 550 (July 2021) 152905.
[12] T. Schwarz-Selinger, Deuterium retention in MeV self-implanted tungsten: influence of damaging dose rate, Nuclear Materials and Energy 12 (August 2017) 683–688.
[13] J.B. Wallace, L.B.B. Aji, L. Shao, S.O. Kucheyev, Dynamic annealing in Ge studied by pulsed ion beams, Sci. Rep. 7 (October 2017).
[14] L.B.B. Aji, J.B. Wallace, L. Shao, S.O. Kucheyev, Non-monotonic temperature dependence of radiation defect dynamics in silicon carbide, Sci. Rep. 6 (August 2016).

[15] "ASTM E521-16, Standard Practice for Investigating the Effects of Neutron Radiation Damage Using Charged-Particle Irradiation," ASTM International, West Conshohocken, PA, 2016.
[16] H. Trinkaus, H. Ullmaier, Conditions for effects of radiation pulsing, J. Nucl. Mater. 307–311 (December 2002) 1705–1709.
[17] N.M. Ghoniem, H. Gurol, An analytical approach to void growth in metals under intense radiation pulsing, Radiat. Eff. 55 (January 1981) 209–221.
[18] H. Gurol, N.M. Ghoniem, Irradiation creep by the climb-controlled glide mechanism in pulsed fusion reactors, Radiat. Eff. 52 (January 1980) 103–125.
[19] J. Le Coze, Procurement of pure fe metal and fe-based alloys with controlled chemical alloying element contents and microstructure, Saint Etienne, France, 2007.
[20] M. Roldán, P. Fernández, R. Vila, A. Gómez-Herrero, F.J. Sánchez, The effect of triple ion beam irradiation on cavity formation on pure EFDA iron, J. Nucl. Mater. 479 (October 2016) 100–111.
[21] T. Tadić, T. Dunatov, S. Fazinić, D.D. Cosic, M. Jakšić, Z. Siketić, M. Vićentijević, W. Kada, C.D. Hardie, Development of the dual-beam ion irradiation Facility for Fusion Materials (DiFU), Materials 16 (January 2023) 1144.
[22] G.S. Was, S. Taller, Z. Jiao, A.M. Monterrosa, D. Woodley, D. Jennings, T. Kubley, F. Naab, O. Toader, E. Uberseder, Resolution of the carbon contamination problem in ion irradiation experiments, Nucl. Instrum. Methods Phys. Res., Sect. B 412 (December 2017) 58–65.
[23] R.E. Stoller, M.B. Toloczko, G.S. Was, A.G. Certain, S. Dwaraknath, F.A. Garner, On the use of SRIM for computing radiation damage exposure, Nucl. Instrum. Methods Phys. Res., Sect. B 310 (September 2013) 75–80.
[24] Y.-R. Lin, S.J. Zinkle, C.J. Ortiz, J.-P. Crocombette, R. Webb, R.E. Stoller, Predicting displacement damage for ion irradiation: origin of the overestimation of vacancy production in SRIM full-cascade calculations, Curr. Opin. Solid State Mater. Sci. 27 (December 2023) 101120.
[25] C. Borschel, C. Ronning, Ion beam irradiation of nanostructures – a 3D Monte Carlo simulation code, Nucl. Instrum. Methods Phys. Res., Sect. B 269 (October 2011) 2133–2138.
[26] M. Roldán, F.J. Sánchez, P. Fernández, C.J. Ortiz, A. Gómez-Herrero, D.J. Rey, Dislocation loop generation differences between thin films and bulk in EFDA pure iron under self-ion irradiation at 20 MeV, Metals 11 (December 2021) 2000.
[27] M. Roldán, F.J. Sánchez, R. Vila, On the strain effect in dislocation loops produced by self-ion irradiation to emulate in-service reactor condition, Nucl. Instrum. Methods Phys. Res., Sect. B 516 (April 2022) 23–30.
[28] W. Jäger, H. Trinkaus, Defect ordering in metals under irradiation, J. Nucl. Mater. 205 (October 1993) 394–410.
[29] Y. Zhang, "A review of void and gas bubble superlattices self-organization under irradiation", Frontiers in nuclear, Engineering 2 (January 2023).
[30] C.A. Schneider, W.S. Rasband, K.W. Eliceiri, NIH image to ImageJ: 25 years of image analysis, Nat. Methods 9 (June 2012) 671–675.
[31] L.K. Mansur, A.D. Brailsford, W.A. Coghlan, A cascade diffusion theory of sink capture fluctuations during irradiation of a solid, Acta Metall. 33 (August 1985) 1407–1423.
[32] A.M. Monterrosa, D. Woodley, Z. Jiao, G.S. Was, The influence of carbon on cavity evolution in ion-irradiated ferritic-martensitic steels, J. Nucl. Mater. 509 (October 2018) 722–735.
[33] Z. Hu, L. Shao, Effects of carbon on void nucleation in self-ion–irradiated pure iron, Nucl. Sci. Eng. 198 (August 2023) 145–157.
[34] L. Malerba, M.C. Marinica, N. Anento, C. Björkas, H. Nguyen, C. Domain, F. Djurabekova, P. Olsson, K. Nordlund, A. Serra, D. Terentyev, F. Willaime, C. S. Becquart, Comparison of empirical interatomic potentials for iron applied to radiation damage studies, J. Nucl. Mater. 406 (November 2010) 19–38.